Wind and Structures, *Vol. 26, No. 2 (2018) 75-87*
DOI: https://doi.org/10.12989/was.2018.26.2.075

Experimental study and FE analysis of tile roofs under simulated strong wind impact

Peng Huang, Huatan Lin, Feng Hu and Ming Gu*

State Key Laboratory of Disaster Reduction in Civil Engineering, Tongji University, Shanghai 200092, China

(Received July 26, 2017, Revised November 29, 2017, Accepted December 21, 2017)

Abstract. A large number of low-rise buildings experienced serious roof covering failures under strong wind while few suffered structural damage. Clay and concrete tiles are two main kinds of roof covering. For the tile roof system, few researches were carried out based on Finite Element (FE) analysis due to the difficulty in the simulation of the interface between the tiles and the roof sheathing (the bonding materials, foam or mortar). In this paper, the FE analysis of a single clay or concrete tile with foam-set or mortar-set were built with the interface simulated by the equivalent nonlinear springs based on the mechanical uplift and displacement tests, and they were expanded into the whole roof. A detailed wind tunnel test was carried out at Tongji University to acquire the wind loads on these two kinds of roof tiles, and then the test data were fed into the FE analysis. For the purpose of validation and calibration, the results of FE analysis were compared with the full-scale performance of the tile roofs under simulated strong wind impact through one-of-a-kind Wall of Wind (WoW) apparatus at Florida International University. The results are consistent with the WoW test that the roof of concrete tiles with mortar-set provided the highest resistance, and the material defects or improper construction practices are the key factors to induce the roof tiles' failure. Meanwhile, the staggered setting of concrete tiles would help develop an interlocking mechanism between the tiles and increase their resistance.

Keywords: tile roof; wind tunnel test; typhoon; wind pressure; FE analysis; displacement

1. Introduction

In the last few years, typhoons have caused a direct economic loss of up to tens of billions of dollars in the world for each year. The investigation of the wind-induced disaster shows that more than half of total losses are related to the damage of low-rise buildings. While most houses suffered little structural damage, many roof coverings were broken, specially the roof tiles. It is important to figure out the wind loads acting on roof tiles and the performance of roof tiles under the loads, not only for reducing property loss of the house and inner facilities but also for the prevention of secondary damages caused by tile debris in strong wind.

In the early studies on this subject, Hazelwood (1980, 1981) studied the wind force on roof tiles laid over a low-permeability underlay, and found that surface flow forces are more severe on windward slope while internal flow forces can be severe on the leeward slope; Kramer and Gerhardt (1983) studied the critical wind loads of two different types of roof systems (tiles on pitched roofs and paving slabs on flat roofs), and found that the critical loading on a roofing element does not necessarily occur for the critical external pressure distribution on the roof surface; Amano *et al.* (1988) described the wind loading mechanism on the blocks with relatively thick air-layers underneath; Gerhardt *et al.* (1990) gave results of experiments and calculations concerning the safety against wind lift-off of loosely laid pavers and insulation boards on flat roofs; Bienkiewicz and Sun (1992, 1997) studied wind loading and resistance of loose-laid roof paver systems and paid attention to distribution of correlation of external and underneath pressure, and found that space between pavers improves the wind resistance of system; Kawair and Nishimura (2003) took field measurements to assess uplift force on hip roof tiles in natural wind; Gavanski *et at*. (2013) examined wind loads on roof sheathing on typical low-rise, wood-frame house for a variety of parameters including the roof shape, roof slope, building height, upstream terrain and the presence of surrounding structures placed in several patterns; Daniel *et al.* (2016) investigated a wind tunnel method for determining wind-induced loads on roof tiles; Habte *et al*. (2017) conducted full-scale experiments to investigate wind loading on roof tiles in hip, ridge, and perimeter locations, and the results show that net uplift was lower than external surface uplift.

Most previous investigations focused on characteristics of wind pressures on the roof tile through the wind tunnel tests and full-scale measurements, while few experiments exist on the uplift resistance of roof tiles and their attachment systems. In addition, though there were lots of works based on FE analysis, they mainly focused on system behavior of the whole building (Pfretzschner *et al*. 2014, Martin *et al*. 2011, Zisis *et al*. 2011 and Pan 2014), and few researches were carried out based on FE analysis for the tile roofs due to the difficulty in the simulation of the interface between the tiles and the roof sheathing (the bonding materials, foam or mortar).

In this paper, a series of laboratory experiments on

*Corresponding author, Professor
E-mail: minggu@tongji.edu.cn

ISSN: 1226-6116 (Print), 1598-6225 (Online)

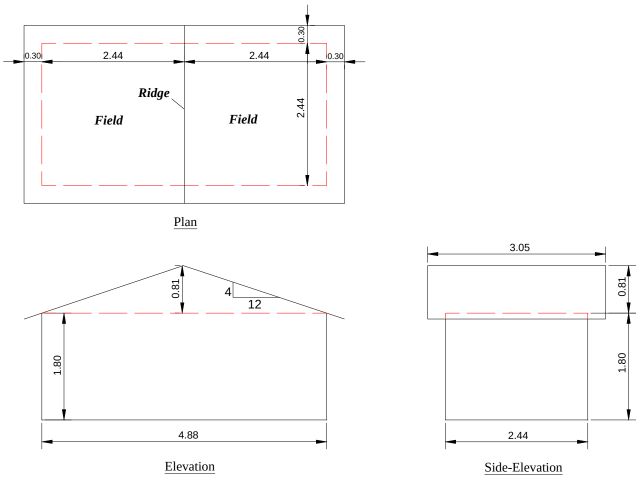

Fig. 1 The prototype size of the house (unit: m)

(a) Clay tile roof (b) Concrete tile roof

Fig. 2 Roof models in wind tunnel

single tiles system were carried out. Based on the mechanical uplift and displacement test data the FE analysis of a single caly or concrete tile with foam-set or mortar-set were built with the interface simulated by the equivalent nonlinear springs. The models were then expanded to the entire roof system, consisting of the field and ridge tiles, the bonding materials, the roof deck, and the roof truss. The general purpose software, ANSYS Version 15.0 was used for the finite element modeling of tile roof system. The model developed in this study can be used for further analysis of various tile roof systems under dynamic and impact loading.

As the pressure points were less and only two wind directions were tested in the WoW tests, a detailed wind tunnel test is carried out at Tongji University to acquire the wind loads on tile roofs, and the results are briefly analyzed. Then, the test data are fed into the finite element model mentioned above. For the purpose of validation and calibration, the results of FE analysis are compared with the performance of tile roofs under simulated typhoon impact through one-of-a-kind Wall of Wind (WoW) apparatus at Florida International University. Finally, some conclusions based on the analysis of this model are obtained.

2. Wind tunnel testing

The tests of the clay and concrete tile roofs aiming to obtain their pressure distributions are conducted in TJ-2 Boundary Layer Wind Tunnel of Tongji University. TJ-2 wind tunnel has a testing section of 3 m in width, 2.5 m in height and 15 m in length with wind velocity ranging from 0.5 m/s to 68 m/s.

Two models are made of PMMA at a geometric scale of 1:5, the prototype size is presented in Fig. 1 and the finished models were shown in Fig. 2. In order to measure the pressures on the ridge and field tiles simultaneously, 357 taps and 379 taps are drilled on the clay and concrete tiles roof, respectively (see Fig. 3). There are 25 wind angles (β) conducted as following: 0°, 10°, 15°, 20°, 30°, 40°, 45°, 50°, 60°, 70°, 75°, 80°, 90°, 100°, 105°, 110°, 120°, 130°, 135°, 140°, 150°, 160°, 165°, 170°, and 180°. A boundary layer flow over open terrain is simulated in the wind tunnel, whose turbulence intensities I_u at the top of the roofs is about 15% in accordance with GB20009-2012(2012) (see Fig. 4). The wind speed at the top of the roof is chosen to be the reference wind speed with a value of 12 m/s. The sampling frequency is 312.5 Hz in this test, and the sampling time is 60 seconds.

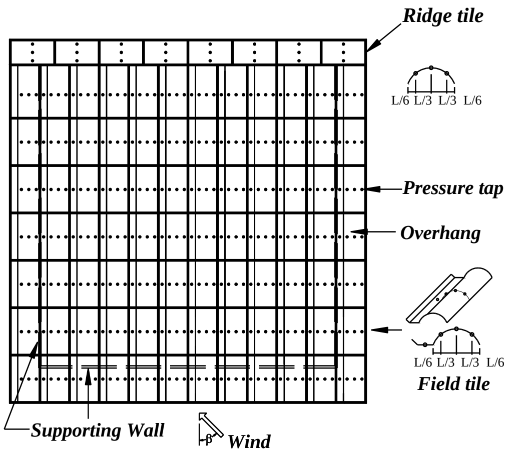

(a) Clay tile roof

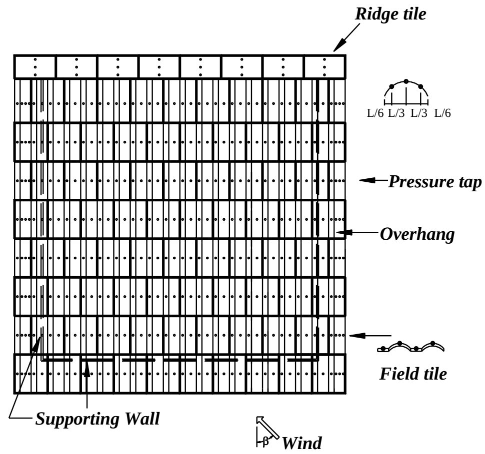

(b) Concrete tile roof

Fig. 3 Pressure taps layout

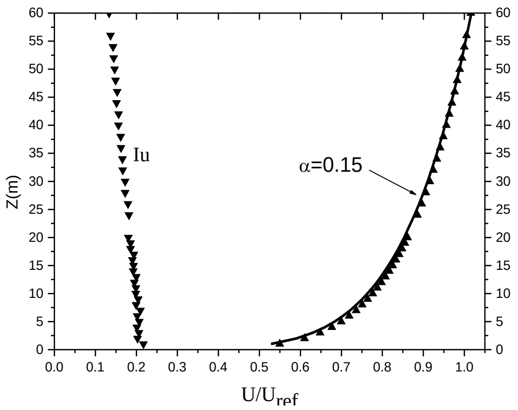

Fig. 4 Mean wind speed and turbulent intensity

The pressure coefficient at the ith tap is estimated as follows

$$C_{Pi} = \frac{P_i - P_\infty}{0.5\rho U^2} \tag{1}$$

Where P_i is the pressure at the ith tap; P_∞ is the static pressure of the Pitot tube; ρ is the air density; and U is the mean wind speed at the top of the roof .The mean, RMS (root mean square), and the maximum and minimum values of C_{Pi} are computed, as bellow

$$C_{Pmean} = \frac{\sum_1^N C_{Pi}}{N} \tag{2}$$

$$\sigma_{Pi} = \sqrt{\frac{\sum_1^N \left(C_{Pi} - C_{Pmean}\right)^2}{N-1}} \tag{3}$$

$$C_{P\max} = C_{Pmean} + \mathrm{G} \cdot \sigma_{Pi} \tag{4}$$

$$C_{P\min} = C_{Pmean} \text{-} \mathrm{G} \cdot \sigma_{Pi} \tag{5}$$

$$\mathrm{G} = \sqrt{2\ln vT} + 0.5772 / \sqrt{2\ln vT} \tag{6}$$

Where N is the total number of samples in each data set, G is the peak factor according to Davenport (1964), v is the cyclic rate, T is the sampling time. Note that Mooneghi *et al*. (2016) provided a professional method to enhance the ability of existing boundary layer wind tunnel facilities to predict full scale wind loads for large scale model. Mooneghi *et al*. (2016) used two methods to predict full scale wind loads: namely PTS method and 3DPTS method. The PTS method, which is simpler to apply, has an accurate prediction for peak coefficients on wall while the prediction for the peak coefficients on roof seem to be inaccurate; and the 3DPTS method requires a number of test at different azimuth and pitch angles at small angle increments around the main wind direction which is unavailable at present. Since this paper is focus on the roof system and test data is limited, so the PTS and 3DPTS methods are both unsuitable in this paper.

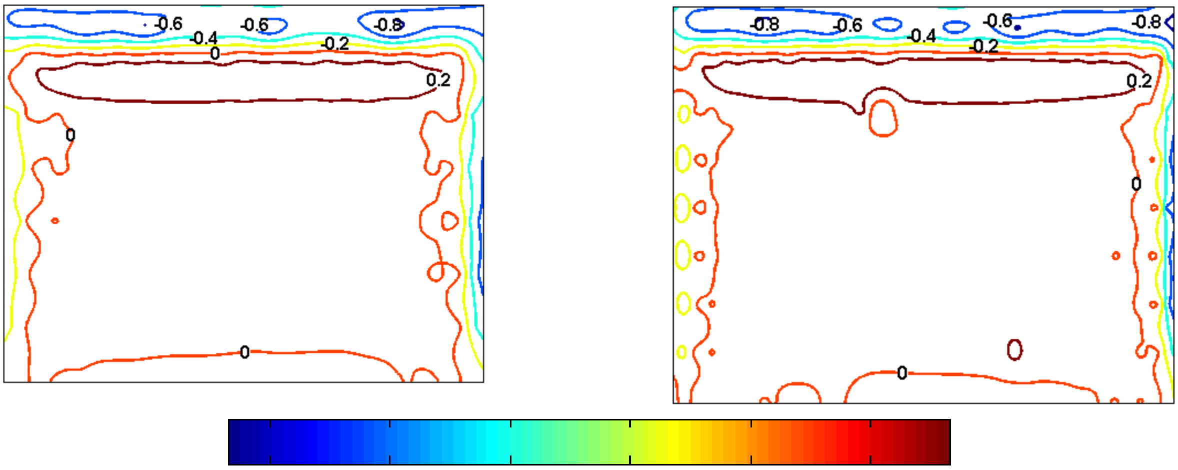

(a) Clay tile roof (b) Concrete tile roof

Fig. 5 Mean pressure coefficient contour of tile roofs in 0° direction

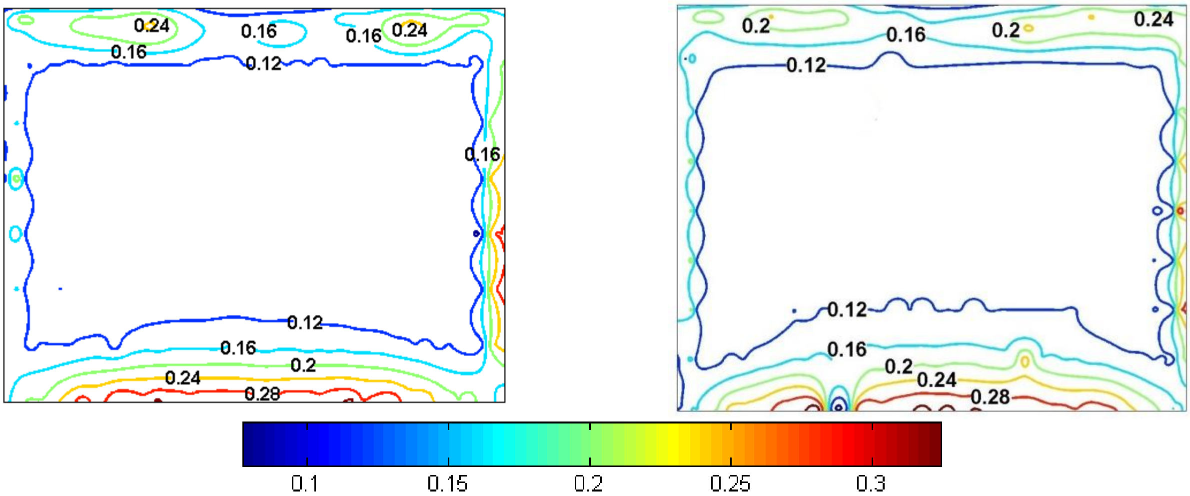

(a) Clay tile roof (b) Concrete tile roof

Fig.6 Fluctuating pressure coefficient contour of tile roofs in 0° direction

For brief introduction, the pressure coefficient contours of the two different tile roofs in two typical wind directions, 0° and 50°, are shown in Figs. 5-8.

Figs. 5 and 6 show the distribution of the mean and fluctuating pressure coefficient in 0° direction on two roofs, respectively. From Fig. 5, most of the mean pressure coefficients on field tiles are close to 0, while there are still two different areas, one is the part close to the ridge tiles with values of about 0.2, and the other is the part in the right side with values of about -0.6. For the ridge tiles, there are positive pressures on the windward surfaces and suctions on the top and leeward surfaces. The minimum negative pressure coefficients on two roofs are both about -0.8, which occur both on the right side of ridge tiles. Overall, the distribution of pressure coefficient presents symmetry under this circumstance. From Fig. 6, the fluctuating pressure coefficients on the edge of the field tiles are larger than those on the middle, and the maximum fluctuating pressures of two roofs are both 0.28, which occur on the eaves. For the ridge tiles, the maximum fluctuating pressures of two roofs are both 0.24.

Figs. 7 and 8 show the distribution of the mean and fluctuating pressure coefficient in 50° direction on two roofs, respectively. From Fig. 7, most of the mean pressure coefficients on field tiles are close to 0.2. Due to the conical vortex in 50° direction on the edge of the roof, the mean and fluctuating pressure coefficients on windward side are much larger than those on other areas. The minimum negative mean pressure coefficients in 50° direction on two roofs are both -2.2, which occur on the top right corner. From Fig. 8, most of the fluctuating pressure coefficients on field tiles are close to 0.1. The maximum fluctuating pressure coefficients on clay and concrete tile roofs are 0.6 and 0.7, respectively, which occur both on the top right corner.

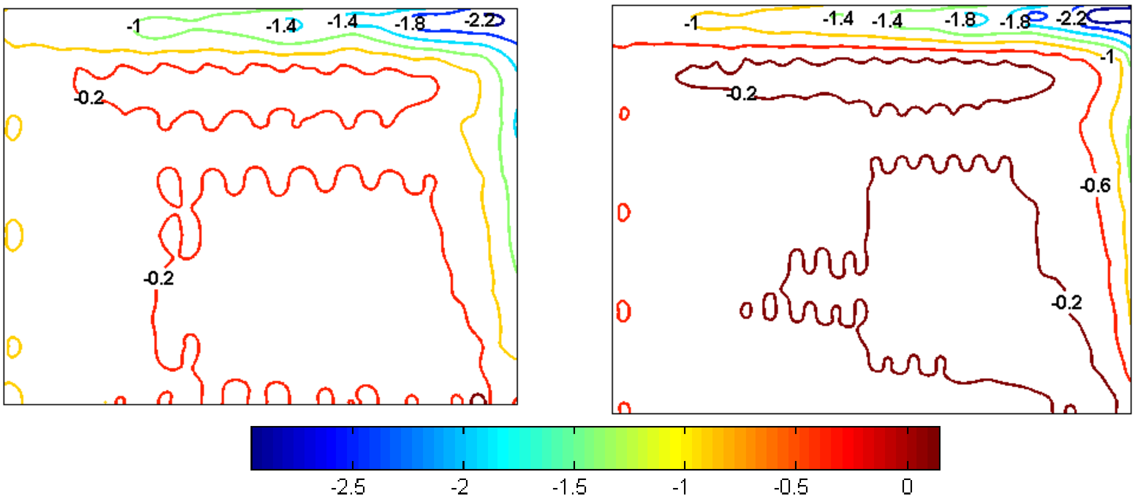

(a) Clay tile roof (b) Concrete tile roof

Fig. 7 Mean pressure coefficient contour of tile roofs in 50° direction

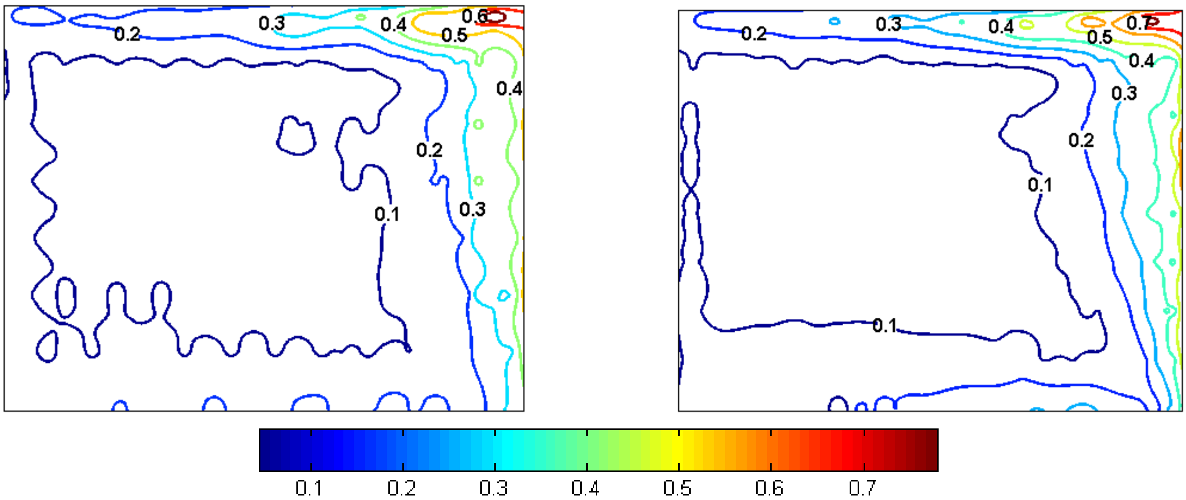

(a) Clay tile roof (b) Concrete tile roof

Fig. 8 Fluctuating pressure coefficient contour of tile roofs in 50° direction

3. FE Modeling and analysis

3.1 Material property of tiles and plywood

Elastic (Young's) modulus of clay and concrete tiles is an important material property in their FE simulations. Coupon tests of clay and concrete tiles were carried out in the laboratory of Florida International University in accordance with ASTM Standard E111-04 (2005), which covered procedures to determine the elastic modulus of clay and concrete tiles. The first author of this paper is one of the main executors of the tests, details are provided in Abi Shdid *et al*. (2011).

Figure 9(a) shows a strip of a concrete tile under axial compression in the lab, with a mounted strain gage. The elastic modulus (E_x) can be calculated, as

$$E_x = \frac{\sigma}{\varepsilon} = \frac{P / A_s}{\varepsilon} \tag{7}$$

Where σ is the axial stress, P is the axial compressive force, A_s is the cross-sectional area of the strip of tile, and ε is the axial strain measured on the tile. Fig. 9(b) shows the measured axial stress-strain response curve by two samples of concrete tiles, leading to an average elastic modulus of 2.08x10^4MPa for concrete tiles. Similar tests on samples of clay tiles led to an average elastic modulus of 1.38 x10^4MPa. The material properties of various components of the roof system are shown in Table 1.

Table 1 Material properties of various components of the roof system

	Clay Tile	Concrete Tile	Wood
Elastic Modulus (Mpa)	1.38x10^4	2.08x10^4	0.83x10^4
Poisson's Ratio	0.20	0.20	0.29
Mass Density (kg/m^3)	1.38x10^3	1.38x10^3	0.55 x10^3
Thickness (mm)	12.7	12.7	12.7

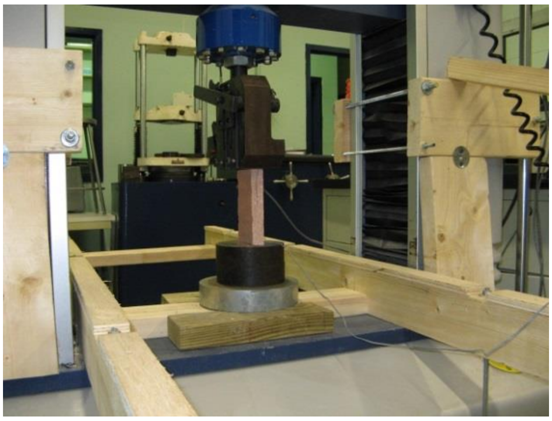

(a) Tile strip under axial compression

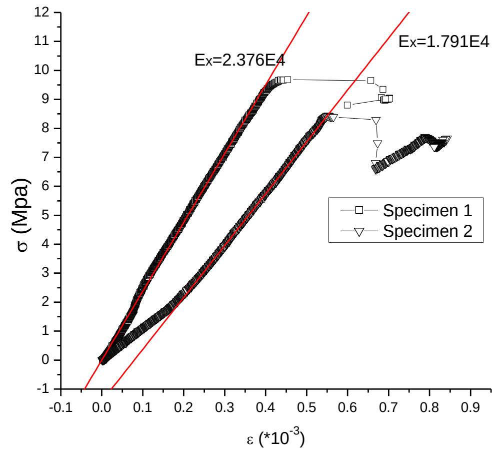

(b) Axial Stress-Strain Response

Fig. 9 Elastic modulus test of concrete tiles

3.2 Material property of interface between tile and plywood board

There are currently two main attachment methods for clay and concrete tiles: foam-set and mortar-set. The interface between the roof tiles and the roof sheathing (the bonding materials, foam or mortar) poses the most challenging issues for finite element modeling. For accurate modeling of the tiles and the interface, a series of laboratory experiments on single tiles system were carried out at Florida International University, more information can be referred to Abi Shdid *et al*. (2011). The mechanical uplift and displacement data are used to calibrate the stiffness coefficients of the equivalent nonlinear springs, which are applied to simulate the interface in the finite element modeling.

3.2.1 Single ridge tile

Taking single clay ridge tile with mortar-set as an example, Fig. 10(a) shows the test set-up for single clay ridge tiles with mortar-set placed on three field tiles that were in turn mechanically attached to a 12.7 mm plywood deck. The figure also presents the positions of potentiometers (Points A~D), where the displacements of the system were measured, and the load-deflection curves are plotted in Fig. 10(b). The stiffness of the interface (equivalent spring) is then calculated based on the difference of the load-deflection response at the center point of the tile (Point A) and the average of the responses at field tile under the ridge tile (Points C and D), i.e., A-(C+D)/2.

The ANSYS model for the clay ridge tile with mortar-set is shown in Fig. 10(c). The clay ridge tiles, as well as the plywood deck, are discretized using elastic shell (Shell63) elements. The ridge tile is meshed using 216 shell elements with 18 and 12 equal divisions in the longitudinal and transverse directions, respectively. The plywood board is affixed at the corners using pin supports. The attachment interface is modeled using 10 nonlinear springs (Combin39) elements which are evenly distributed in the middle of ridge tile along the longitudinal axis, and the restraint and the beam element in the middle of plywood board are considered as simplified model to provide connection for the equivalent spring for ridge tile. The nonlinear stiffness coefficients of single nonliear spring used in the model for mortar-set are shown in Fig. 10(d). The load is applied at the center of the tile to simulate the mechanical uplift tests. Comparisons of the ANSYS model simulation with the test are shown in Fig. 10(e), which indicate good agreement.

For the single ridge tile with foam-set (foam), similar process is carried out. Details are provided in Mirmiran *et al*. (2007).

3.2.2 Single field tile

Taking single clay field tile with foam-set as an example, the single clay field tile is attached with foam to a hot mopped 30/90 deck underlayment, and a 12.7 mm plywood decking. Fig. 11(a) shows the locations of potentiometers (Points 1~4), where displacements of the system were measured. The clay field tile is meshed using 288 elements with 18 and 16 equal divisions in the longitudinal and transverse direction, respectively. The plywood board is affixed at the corners using pin supports. The ANSYS model for the clay field tile with foam-set is shown in Fig. 11(b).

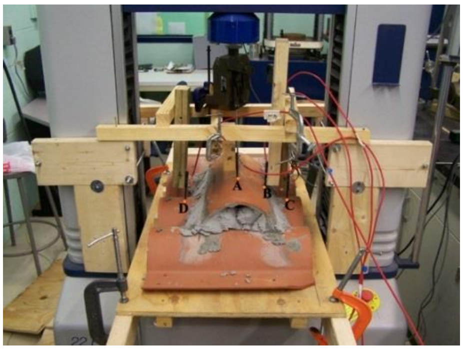

(a) Clay ridge tile with mortar-set

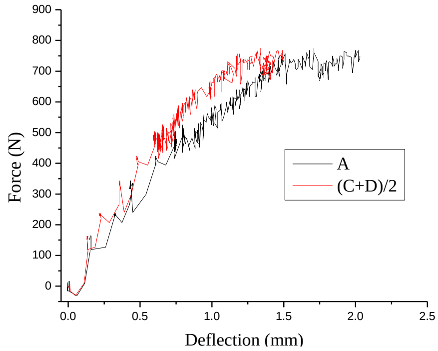

(b) Load-deflection curves

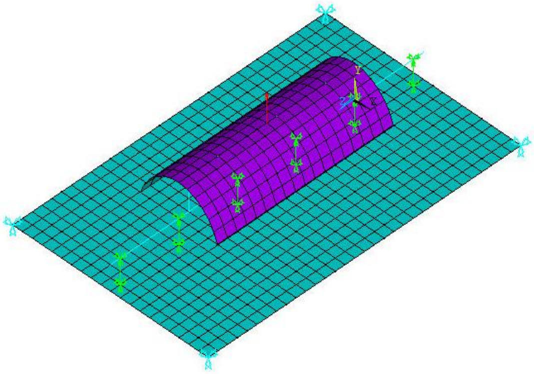

(c) Ansys model

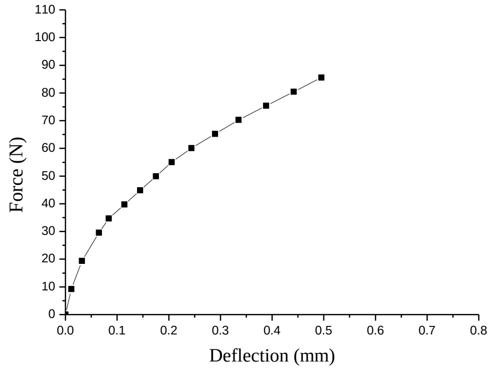

(d) Nonlinear spring parameters

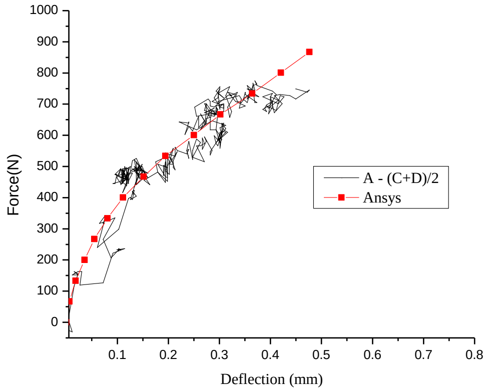

(e) Comparison of the load-deflection in ANSYS and in test

Fig. 10 Modeling of single clay ridge tile system with mortar-set

The interface is simulated by 16 nonliear spring which are divided into two rows and evenly distributed in the location of interface. The parameters of nonliear spring shown in Fig. 11(d) are manually debugged until the load-deflections of point 1 to 4 in the FE analysis coincide well with the test data, which are shown in Fig. 11(c). It is clear that the results of the FE analysis coincide well with the test data, so the equivalent spring parameters are calibrated to be correct. The equivalent springs' constants for other set-up of single tile systems are shown in Fig. 12.

From Fig. 12(a), it is clear that concrete field tile with mortar has the largest stiffness and resistance capacity; clay field tile with mortar has the worst stiffness and resistance capacity; the stiffness and resistance capacity of clay field tile with foam are slightly larger than that of concrete field tile with foam. From Fig. 12(b), the concrete ridge tile with mortar and clay ridge tile with foam also have the larger stiffness and resistance capacity with that of concrete ridge tile with foam and clay ridge tile with mortar; while the stiffness of concrete ridge tile with foam is smaller than clay ridge tile with mortar which is contrary to the field tile.

3.3 Modeling and analysis of entire tile roof system

Based on the above-mentioned calibration data of single ridge and field (clay and concrete) tiles with foam-set and mortar-set, the finite element model for a large section of the roof system (see Fig. 13) is established to simulate the effects of wind loads and to compare the calculated results with the Wall of Wind (WoW) test data. The complete roof model consists of field and ridge tiles, attachment materials, roof deck, and the roof trusses. Note that the roof trusses are set to provide brace for plywood board. The staggered setting is also simulated in the model. As shown in Fig. 3,

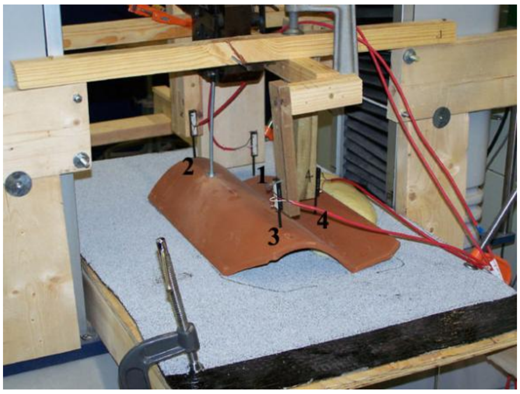

(a) Clay field tile with foam-set

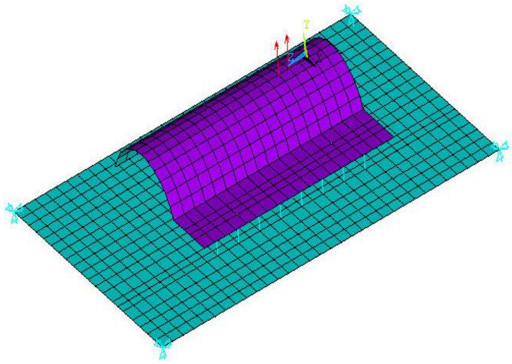

(b) Ansys model

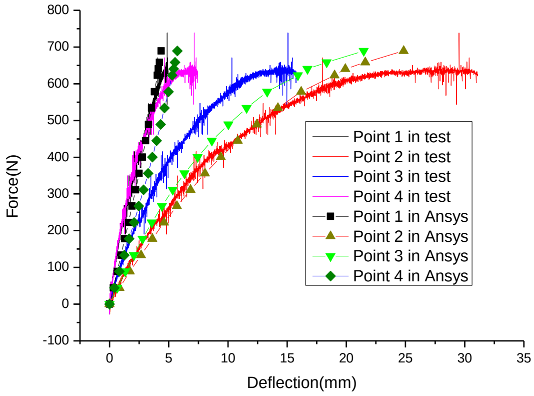

(c) Load-deflection curves

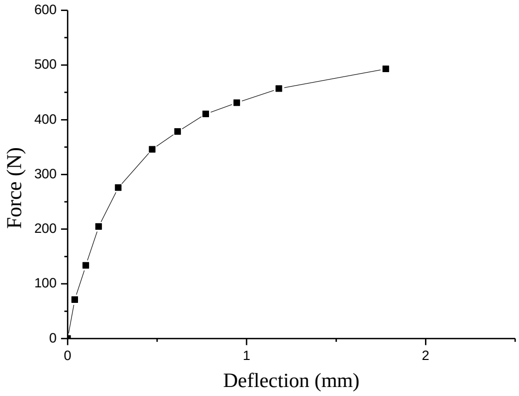

(d) Nonlinear spring parameters

Fig. 11 Modeling of single clay field tile system with foam-set

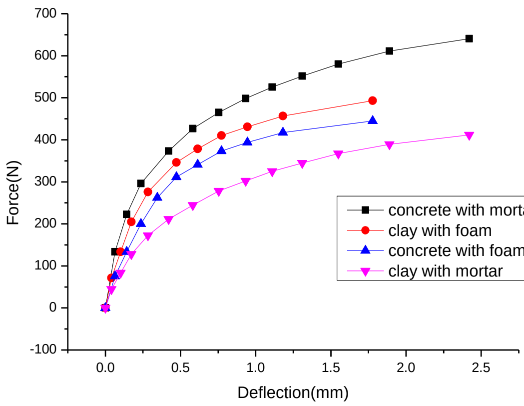

(a) Field tile

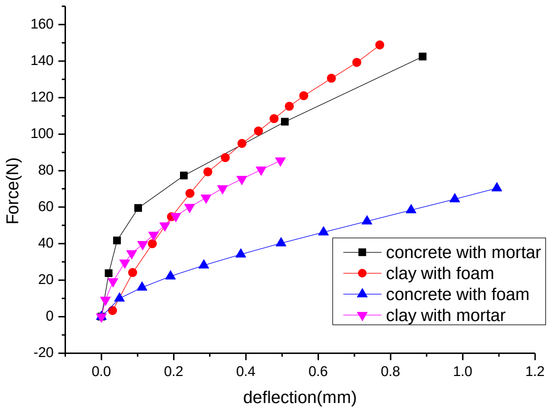

(b) Ridge tile

Fig. 12 ANSYS nonlinear spring parameters

concrete field tiles are installed in a staggered pattern while the clay field tiles are installed in tandam. The clay and concrete tiles, as well as the plywood deck, are discretized using elastic shell (Shell63) elements. The truss members are modeled using three-dimensional beam (Beam4) elements. The interface between the roof tiles and the plywood deck, i.e., the foam or mortar, is finally built using nonlinear spring (Combin39) elements.The ANSYS model for the entire clay tile roof is meshed with 11,481 nodes and 12,569 elements while the concrete tile roof is 13,681 nodes and 14,146 elements.

The wind loads obtained in the wind tunnel tests are applied to the models to carry out the finite element analysis. Wind load are implemented on tiles as a concentrated force, the magnitude is depending on the coefficient and its tributary area. The quasi-steady analysis is conducted, and the load is varying in space depending on the force coefficients tested in the wind tunnel. The analysis results are compared with the full-scale performance of tile roofs under simulated typhoon impact through one-of-a-kind Wall of Wind (WoW) apparatus.

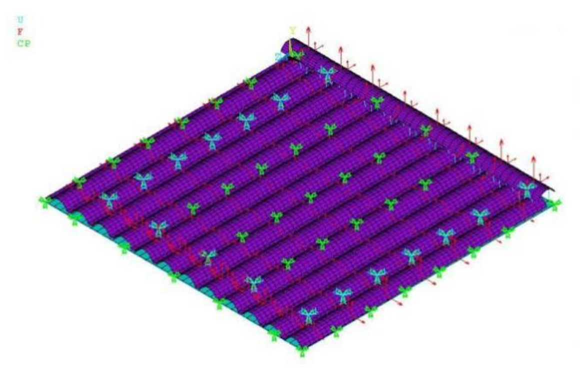

(a) Clay tile roof

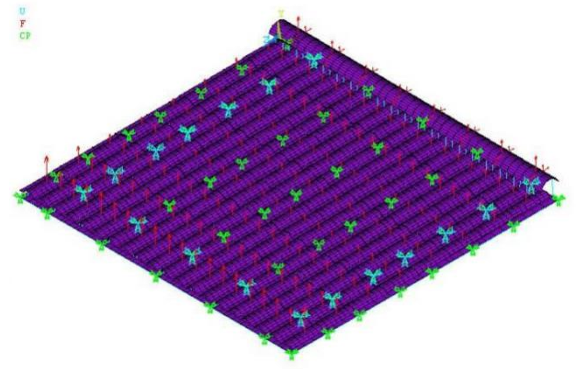

(b) Concrete tile roof

Fig. 13 Ansys model of entire tiles roof system

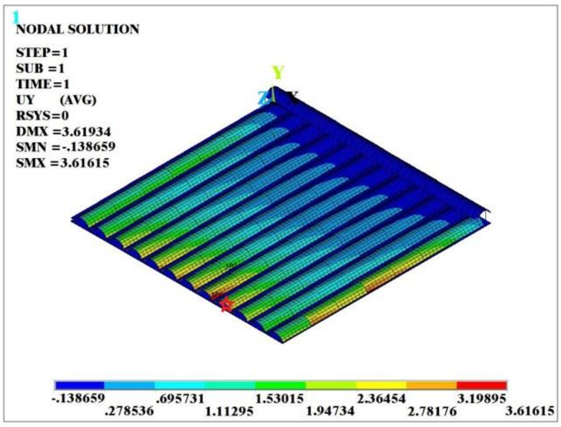

(a) Clay tile roof (0°direction)

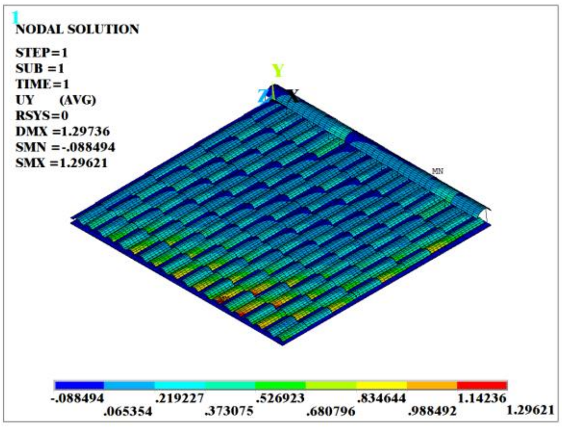

(b) Concrete tile roof (0° direction)

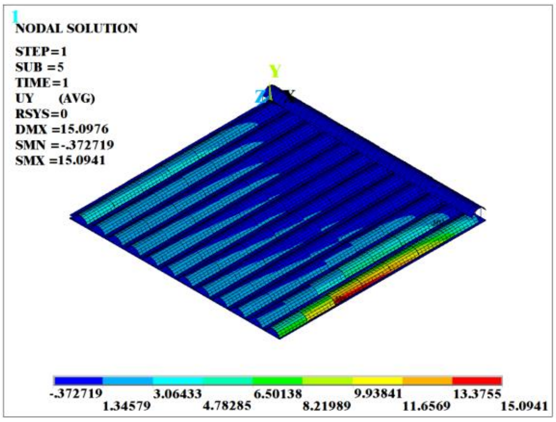

(c) Clay tile roof (50° direction)

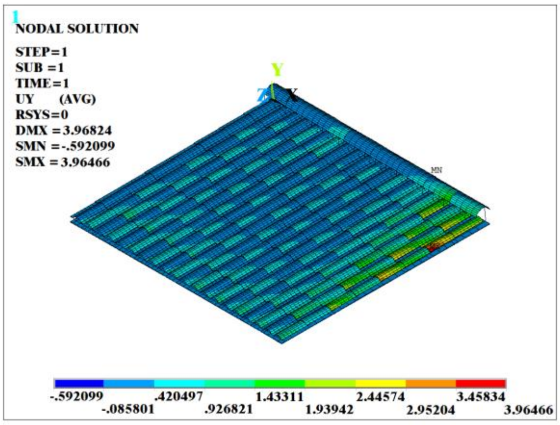

(d) Concrete tile roof (50° direction)

Fig. 14 Vertical displacements on tile roofs with mortar-set (unit:mm)

The results of the Wind Tunnel Testing and the Wall of Wind Testing showed that the roofs were mainly affected by the suctions, so the minimum pressure coefficients ($C_{P\min}$) are used to calculate the wind loads on field and ridge tiles.

4. Results and discussions

The wind loads obtained in section 3 are fed into the finite element model for calculation, the responses of the finite element model including internal force, displacement, relative displacements are obtained. The reliability of FE analysis is validated by comparing to the data of WOW.

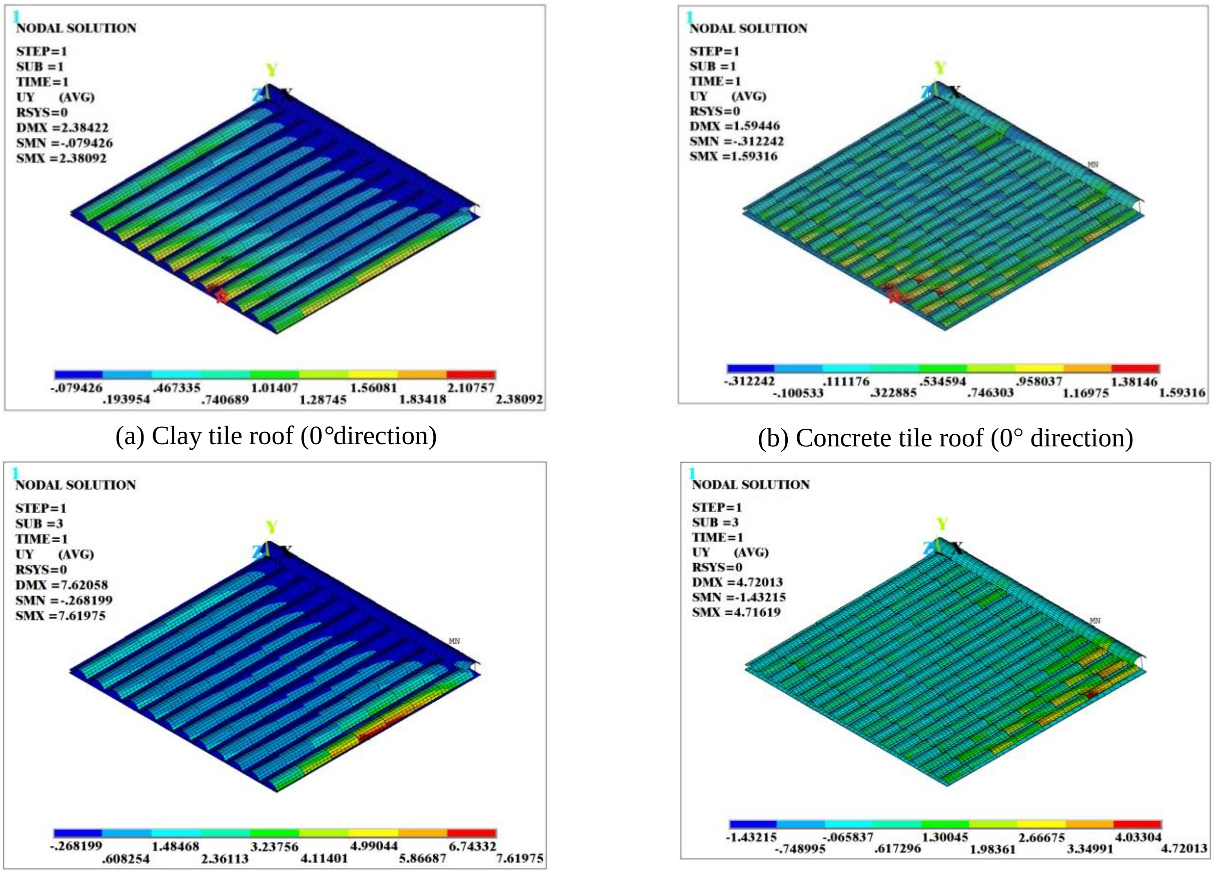

(a) Clay tile roof (0°direction)

(b) Concrete tile roof (0° direction)

(c) Clay tile roof (50° direction)

(d) Concrete tile roof (50° direction)

Fig. 15 Vertical displacements on tile roofs with foam-set (unit: mm)

The detail results and discussions are shown below:

Fig, 14 shows the contours of vertical displacement on clay and concrete tile roofs with mortar-set at wind speed of 53.64 m/s (120 miles/hour) in the 0° and 50° wind directions, respectively. In the 0° direction, the maximum displacement occurs on the eave with a value of 1.3 mm in concrete tile roof and 3.6 mm in clay tile roof, respectively.

In the 50° direction, the large displacement occurs on the right side due to conical vortex. For the clay tile roof, the maximum displacement occurs on the third tile with a value of 15.1 mm, while the maximum displacement on the concrete tile roof is 4.0mm which occurs on the seventh tile.

Fig. 15 shows the contours of vertical displacement on clay and concrete tile roofs with foam-set at wind speed of 53.64 m/s in the 0° and 50° wind directions, respectively.

The distributions of the displacement of the foam-set roof are similar with those of the mortar-set roof. In the 0° direction, the maximum displacement occurs on the eave with a value of 1.6 mm in concrete tile roof and 2.4 mm in clay tile roof, respectively. In the 50° direction, the maximum displacement on the clay tile roof is 7.6 mm which occurs on the fourth tile, while the maximum displacement on concrete tile is 4.7mm which occurs on seventh tile.

The failure of the tiles is mainly due to the breakage at the interface. Therefore, for a tile to remain intact, the relative displacement, i.e., the deformations of the equivalent springs (simulating the interface), should be within the range of their respective load-deflection curves. While the tile is remain intact but in a “yield stage”, i.e., a small account of force will lead to a large displacement, the tile can also be considered as dangerous. The deformations of the equivalent springs between the tile and the roof deck are presented in Fig. 16. Figs. 16 show the relative displacement of the roofs with mortar-set and foam-set in the 50° wind directions, respectively. The distributions of relative displacements are similar to those of vertical displacements in Figs. 14 and 15. The largest relative displacements in the 50° wind directions of clay with foam, clay with mortar, concrete with foam and concrete with mortar are 0.8 mm, 1.8 mm, 0.7 mm and 0.5 mm, respectively. It can be seen that the relative displacement is one order of magnitude smaller than the absolute displacement, which shows that the deformation of tile is primarily caused by warping around the bonding site. Fig. 17 shows the states of field tile’s nonliear springs (the one with the largest relative displacement) of four roof systems in the 50° wind directions. Though all relative displacements are within the range of their own load-deflection curves, the clay with foam, clay with mortar and concrete with foam have entered the “yield stage”, which

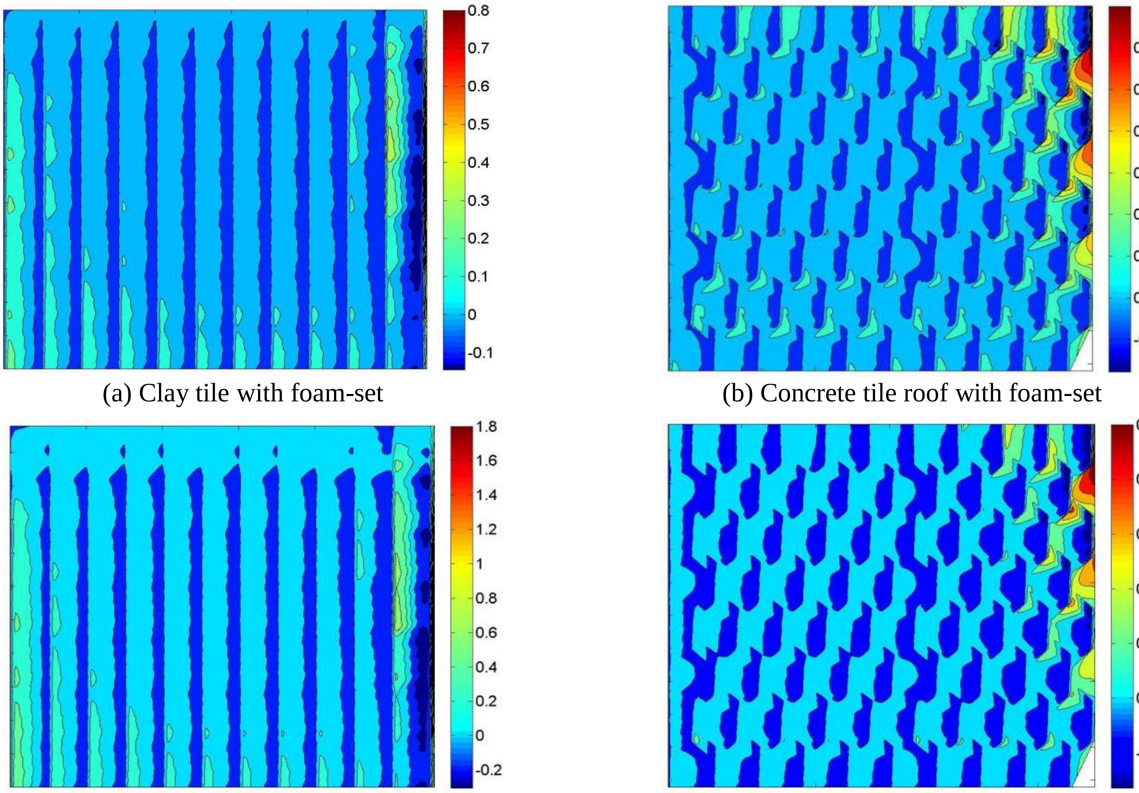

(a) Clay tile with foam-set

(b) Concrete tile roof with foam-set

(c) Clay tile roof with mortar-set

(d) Concrete tile roof with mortar-set

Fig. 16 Relative displacement between the tiles and the sheathing in 50°direction (unit: mm)

means these three type of roofs are almost near the edge of their ultimate resistance capacity. What is more, as displacement became larger, the air enters the cavity of the tile, and the net pressure may increase, so the clay with foam, clay with mortar and concrete with foam are more likely to damage. In general, according to the results of displacement and relative displacement in the FE analysis, it can also be concluded the wind resistance capacity in order from large to small are concrete tile with mortar-set, concrete tile with foam-set, clay tile with foam-set, and clay tile with mortar-set.

Due to the limited full-scale experiment data of the whole roof under strong wind impact, there are only two indexes can be used to be compared: one is the wind resistance of the roof system, and the other is the location where the damage began. For the wind resistance of roof systems, the results in the FE analysis agree well with the result of the WoW test. According to Huang *et al*. (2009), the roof of concrete tile with mortar-set, which has the minimum displacement in the FE analysis, is the only roof remain intact in the WoW test, and the roof of clay tile with mortar-set, which has the largest displacement in the FE analysis, is the roof suffered the greatest damage with almost all of the tiles being destroyed in the WoW test. If the damage area in the WoW test is assumed to be an index to judge the wind resistance of the roof, the wind resistance capacity in order from large to small are concrete tile with mortar-set, concrete tile with foam-set, clay tile with foam-set, and clay tile with mortar-set, which coincide with the order of the displacement and relative displacement in the FE analysis. In addition, those three roof systems broken in the WoW test also enter the dangerous phase in the FE analysis. What is more, it is also found that the place where the maximum displacement occurred in the finite element model was just the place where the damage began in the WoW test, when contours of vertical displacement of roofs were compared to the results in Huang *et al*. (2009). Note that the conspicuous pentagram mark in Figs. 14 and 15 is the location where max displacement occurs in the FE analysis corresponding to the location where the damage began in the WoW test.

The performance of roofs can be explained by the characteristics of the nonlinear springs used in the FE system. It is obvious from Fig. 12(a) that the nonlinear spring of a single clay tile with mortar-set has the worst the wind resistance and the nonlinear spring of a single concrete tile with mortar-set has the best wind resistance. Fig. 12(a) also shows that the deformation of spring of concrete tile with foam-set is larger than that of the concrete tile with mortar-set, which accounts for the larger displacement of the former in the FE analysis. But there is still an abnormal phenomenon that the roof of clay tile with foam-set has a larger displacement than the roof of concrete tile with mortar-set, while the nonlinear springs of a single clay tile with foam-set has the larger stiffness and uplift capacity than that of the concrete tile with foam-set. This phenomenon may attribute to the different setting of these tiles. As mentioned above, the concrete field tiles were

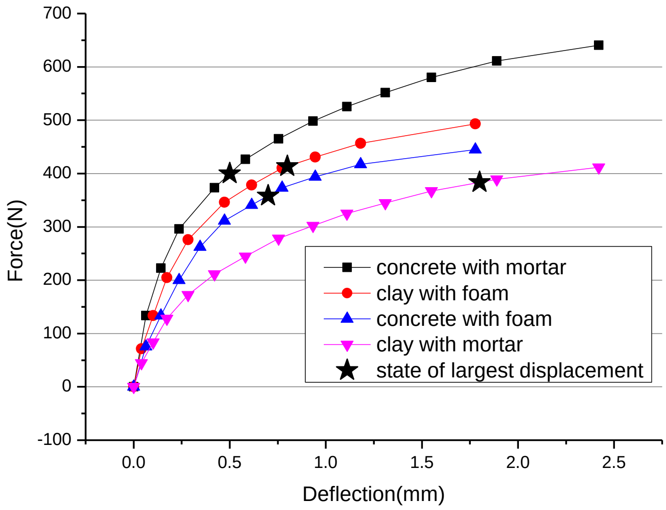

Fig. 17 The states of nonliear springs of four roof systems in the 50° wind directions

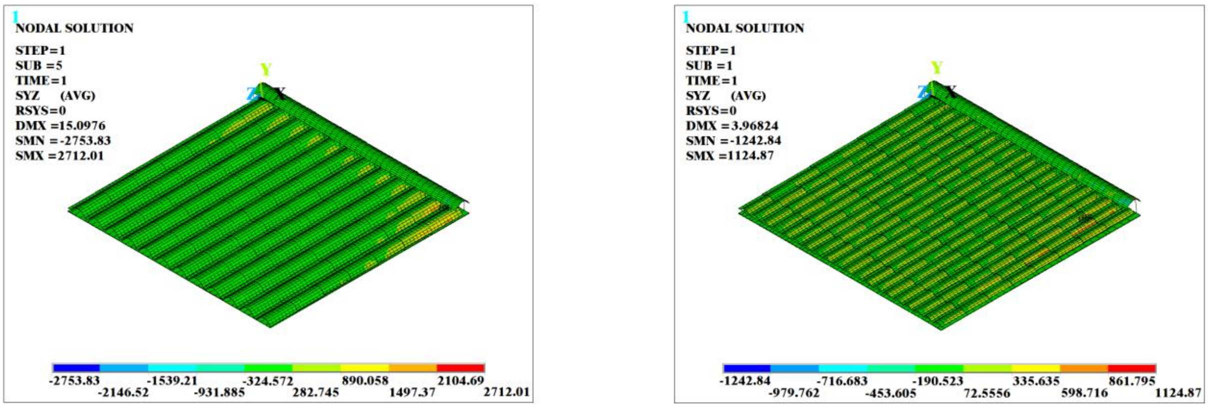

(a) Clay tile roof (b) Concrete tile roof

Fig. 18 Shear stresses on tile roofs with mortar-set in 50° direction(unit:N)

installed in a staggered pattern while the clay field tiles were installed in tandem. The staggered pattern of concrete filed tiles helps form an interlocking mechanism to resist the wind pressure. In order to better understand how the staggered pattern can increase the wind resistance and reduce the deformation, the shear stresses on clay and concrete tile roofs with mortar-set at wind speed of 53.64m/s in the 50°direction were extracted and shown in Fig.18. The shear stresses on the concrete tile roofs are much smaller than that of the clay tile roofs. The roofs with foam-set have the similar calculation results.

An interesting point needs to be noted is that the minimum negative pressure on the ridge tile is almost twice that of the field tile, while the ridge tile has smaller displacement in FE analysis. This may attribute to the different location and different shape of the bonding material between the tiles with plywood which was shown in Abi Shdid *et al*. (2011). The field tile is easier to warp around the bonding site and the deformation of tile is mainly caused by the warping as mentioned above, which accounts for the larger displacement for the field tile in FE analysis.

5. Conclusions

In this study, a detailed wind tunnel testing was carried out at Tongji University, and the wind loads on clay and concrete roof tiles were acquired. The test data were then fed into several FE models of the roof structures, and some important conclusions could be generalized as following:

- The roof systems were found that concrete tile with mortar-set roof provided the highest resistance under typhoon impact, while the clay tile with mortar-set roof provided the worst resistance.
- The eave was the most vulnerable portion on the windward side of the roof, which indicated the edge of the roof should be reinforced specially.
- Though a typhoon impact with speed of 53.64 m/s does not lead to direct damage of the roofs in FE analysis, the roof systems of clay with mortar, clay with foam and concrete with foam are in a dangerous phase.
- Staggered setting of tiles would help develop an interlocking mechanism between the tiles and increase their resistance to typhoon.

Further analysis of various tile roof systems' performance under dynamic and impact loading could be conducted on the base of the finite element model established in this paper.

Acknowledgments

This study was jointly supported by Chinese National Natural Science Foundation (51678452, 51378396), which is gratefully acknowledged. This work was partially supported by the International Hurricane Research Center at Florida International University (FIU), USA, and the helps from Dr. Amir Mirmiran and Dr. Arindam Gan Chowdhury of FIU during the course of the material property tests of the roof tiles are really appreciated.

References

Abi Shdid, C., Mirmiran, A., Wang, T.L., Jimenez, D., and Huang, P. (2011), "Uplift capacity and impact resistance of roof tiles", *ASCE Practice Periodical on Structural Design and Construction*, **16**(3), 121-129.

Amano, T., Fujii, K. and Tazaki, S. (1988), "Wind loads on permeable roof-blocks in roof insulation systems", *J. Wind Eng. Ind. Aerod.*, **29**, 39-48.

ASTM E111-04(2004), Standard Test Method for Young's Modulus, Tangent Modulus and Chord Modulus, ASTM International; West Conshohocken, United States.

Bienkiewicz, B. and Sun, Y. (1992), "Wind-tunnel study of wind loading on loose-laid roofing systems", *J. Wind Eng. Ind. Aerod.*, **41-44**, 1817-1828.

Bienkiewicz, B. and Sun, Y. (1997), "Wind loading and resistance of loose-laid roof paver systems", *J. Wind Eng. Ind. Aerod.*, **72** (1), 401-410.

Daniel, J.S., Forrest, J.M. and Arindam, G.C. (2016), "Investigating a wind tunnel method for determining wind-induced loads on roofing tiles", *J. Wind Eng. Ind. Aerod.*, **155**, 47-59

Davenport A.G. (1964), "Note on the distribution of the largest value of a random function with application to gust loading [C]" *Proceedings of the Institution of Civil Engineers*, paper N0.6739.28, 187-196

FEMA. (2005), "Tile roofing for high-wind area", Rep.499, Washington, DC

Gavanski, E., Kordi, B., Kopp, G.A. and Vickery, P.J. (2013), "Wind loads on roof sheathing of houses", *J. Wind Eng. Ind. Aerod*., **114**, 106-121

Gerhardt, H.J., Kramer, C. and Bofah, K.K. (1990), "Wind loading on loosely laid pavers and instruction boards for flat roofs", *J. Wind Eng. Ind. Aerod.*, **36**, 309-318

GB 50009-2012(2012), Load code for design of building structures, Ministry of Housing and Urban-Rural Construction ofthe People's Republic of China; Beijing, China.

Hazelwood, R.A. (1980), "Principles of wind loading on tiled roofs and their application in the British standard BS5534", *J. Wind Eng. Ind. Aerod.*, **6**, 113-124.

Hazelwood, R.A. (1981), "The interaction of the two principal wind forces on roof tiles", *J. Wind Eng. Ind. Aerod.*, **8**, 39-48.

Habte, F., Mooneghi, M.A., Baheru, T., et al. (2017), "Wind loading on ridge, hip and perimeter roof tiles: A full-scale experimental study", *J. Wind Eng. Ind. Aerod.*, **166**, 90-105.

Huang, P., Mirmiran, A., Gan Chowdhury, A., Abishdid, C. and Wang T.L. (2009), "Performance of roof tiles under simulated Hurricane impact", *J. Architect. Eng.*, **15**(1), 26-34.

Kawair, H. and Nishimura, H. (2003), "Field measurement on wind force on roof tiles", *Proceedings of the 11th Int'l Conf. Wind Engrg.*, Lubbock, U.S.

Kramer, C. and Gerhardt, H.J. (1983), "Wind loads on permeable roofing systems", *J. Wind Eng. Ind. Aerod.*, **13**, 347-358.

Martin, K.G., Gupta, R., Prevatt, D.O., Datin, P.L. and van de Lindt J.W. (2011) "Modeling system effects and structural load paths in a wood-framed structure", *J. Architect. Eng.*, **17**(4), 134-143.

Mirmiran, A., Abishdid, C., Wang, T.L., Huang, P., Jiménez, D.L., and Younes, C. (2007), "Performance of Tile Roofs under Hurricane Impact − Phase 2", Rept. No. SCL – 070801, Dept of Civil and Environ. Engrg., Florida International University, Miami, FL.

Mooneghi M.A., Irwin P. and Chowdhury A.G. (2016), "Partial turbulence simulation method for predicting peak wind loads on small structures and building appurtenances", *J. Wind Eng. Ind. Aerod.*, **157**, 47-62.

Pan, F., Cai, C.S., Zhang, W. and Kong, B. (2014), "Refined damage prediction of low-rise building envelope under high wind load ", *Wind Struct*., **18**(6), 669-691.

Pfretzschner, K., Gupta, R. and Miller, T. (2014), "Practical modeling for wind load paths in a realistic light-frame wood house", *J. Perform. Constr. Fac.*, **28**(3), 430-439.

Zisis, I. and Stathopoulos, T. (2012), "Wind load transfer mechanisms on a low wood building using full-scale load data", *J. Wind Eng. Ind. Aerod.*, **104-106**, 65-75.

AD